Current Mechanisms in VLWIR $Hg_{1-x}Cd_xTe$ Photodiodes

A.I. D'SOUZA,[1] R.E. DEWAMES,[2] P.S. WIJEWARNASURIYA,[2] G. HILDEBRANDT,[2] and J.M. ARIAS[2]

1.—Boeing Sensor & Electronic Products, 3370 Miraloma Avenue, Anaheim, CA 92803; e-mail: arvind.i.d'souza@boeing.com. 2.—Rockwell Science Center, 1049 Camino Dos Rios, Thousand Oaks, CA 91360

VLWIR (λ_c ~ 15 μm to 17 μm at 78 K) detectors have been characterized as a function of temperature to determine the dominant current mechanisms impacting detector performance. $I_d - V_d$ curves indicate that VLWIR detectors are diffusion limited in reverse and near zero bias voltages down to temperatures in the 40 K range. At 30 K the detectors are limited by tunneling currents in reverse bias. Since the detectors are diffusion limited near zero bias down to 40 K, the R_oA_{imp} versus temperature data represents the diffusion current performance of the detector as a function of temperature. The detector spectral response measurement and active layer thickness are utilized to calculate the HgCdTe layer x value and the optical activation energy $E_{a\ optical}$. The activation energy, $E_{a\ electrical}$, obtained from the measured diffusion limited R_oA_{imp} versus temperature data is not equal to the activation energy, $E_{a\ optical}$, obtained from the spectral response measurement for all x values measured. $E_{a\ electrical} = \beta^* E_{a\ optical}$, where β ranges between 0.64 and 1.0 For cutoff wavelengths in the ≤ 9 μm at 78 K, $E_{a\ electrical} = E_{a\ optical}$. $E_{a\ electrical} = 0.65^* E_{a\ optical}$ have been measured for λ_c = 17 μm at 78 K detectors. As the band gap energy decreases to values in the range of 70 meV and lower, it is reasonable to expect a more dominant role of band tailing effects on the transport properties of the material system. In such a picture, one would expect the optical band gap to be unmodified, whereas the intrinsic concentration could be enhanced from its value for the ideal semiconductor. Such a picture could explain the observed behavior. Further probing experiments and modeling efforts will help clarify the physics of this behavior.

Key words: Molecular beam epitaxy (MBE), VLWIR HgCdTe

INTRODUCTION

$Hg_{1-x}Cd_xTe$ material lends itself to the fabrication of high quantum efficiency detectors. The bandgap of $Hg_{1-x}Cd_xTe$ material can be easily tuned from the very short wave infrared (VSWIR—λ_c = 1–2 μm) to the very long wave infrared (VLWIR—λ_c ~ 14–17 μm). This bandgap tunability coupled with the high quantum efficiency obtained in $Hg_{1-x}Cd_xTe$ detectors results in $Hg_{1-x}Cd_xTe$ being extensively utilized for a range of infrared imaging and sounding applications.

Infrared imaging radiometers and sounders require VLWIR (λ_c > 15 μm) detectors. It is, therefore, important to understand the current mechanisms that impact detector performance in these VLWIR detectors. Advances in the molecular beam epitaxy (MBE) growth of HgCdTe and p-on-n double layer planar heterostructure (DLPH) photovoltaic (PV) detector architecture have resulted in producing high performance detectors for infrared focal plane arrays (IRFPAs). MBE is used to grow in-situ double layers; VLWIR $Hg_{1-x}Cd_xTe$ base layer followed by wider bandgap cap layer. Layers discussed here were grown on (211)B lattice-matched CZT substrates. Detectors with p-type implants ranging in size from 8 μm in diameter to 250 μm × 250 μm square were fabricated.[1,2]

(Received November 21, 2000; accepted January 13, 2001)

VLWIR DETECTOR RESULTS

Optical Measurements

$Hg_{1-x}Cd_xTe$ material transmission measurements at room temperature are combined with processed material detector spectral measurements at cryo-

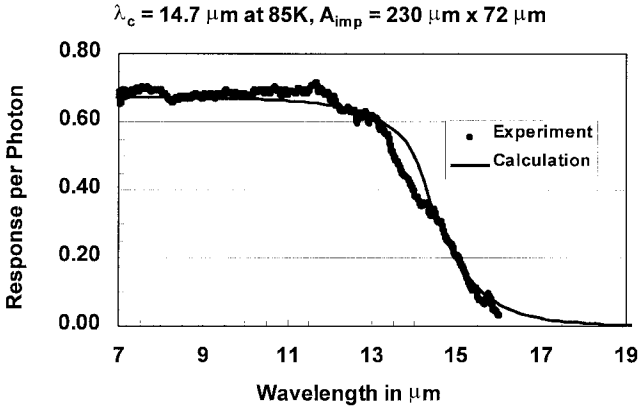

Fig. 1. Quantum efficiency versus wavelength for a λ_c = 15 μm at 78 K detector.

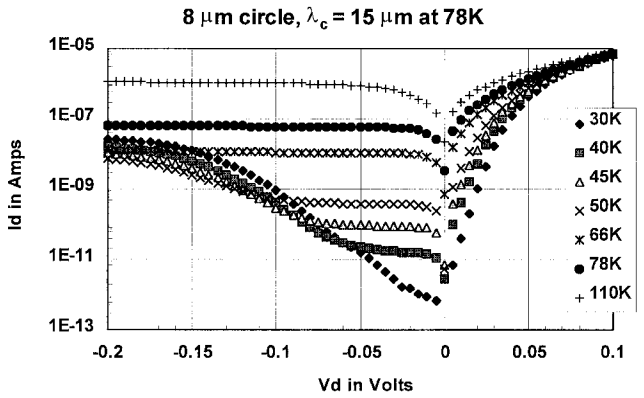

Fig. 2. $I_d - V_d$ curves versus temperature for an 8 μm diameter, λ_c = 15 μm detector.

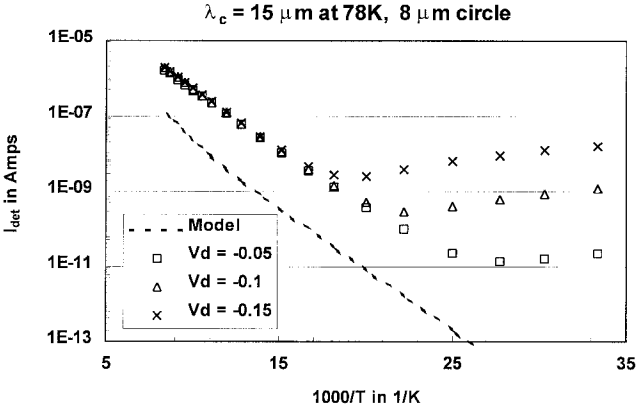

Fig. 3. Dark current versus temperature at –50 mV, –100 mV, and –150 mV detector bias.

genic temperatures to extract the material x value. A Fourier transform infrared spectrometer is used to measure transmission versus wavelength for the layer, yielding material x value and thickness information. Following $Hg_{1-x}Cd_xTe$ detector processing, the spectral response and quantum efficiency of the detector is measured. A modeled[3] and measured quantum efficiency versus wavelength curve is displayed in Fig. 1 for a λ_c = 14.7 μm at 85 K (λ_c = 15.0 μm at 78 K) detector. The measured HgCdTe active layer thickness, detector cutoff wavelength, λ_c, are input parameters to the model. The x_{opt} value is a fitting parameter that best replicates the shape of the measured spectral response or quantum efficiency versus wavelength characteristics of the detector. An $x_{opt} = 0.1997$ was extracted from the quantum efficiency versus wavelength displayed in Fig. 1. The x_{opt} values for all the layers were extracted in this manner. The x_{opt} value thus extracted determines the bandgap at any temperature via the Hansen, Schmit, Casselman equation,[4]

$$E_g(x,T) = -0.302 + 1.93x - 0.81x^3 + 0.832x^3 + 5.35\times10^{-4}T(1-2x) \quad (1)$$

$I_{det} - V_{det}$ versus Temperature

$I_{det} - V_{det}$ versus temperature curves for an 8 μm circle (λ_c = 15 μm at 78 K) detector is displayed in Fig. 2. For small bias values, the detector is diffusion limited when T > 40 K. Analysis of the T = 50 K $I_{det} - V_{det}$ curve for low bias values in the forward and reverse direction, results in an ideality factor n = 1.01, proving that the detector is diffusion limited near zero bias. The dark current values at V_{det} = –50 mV, –100 mV, and –150 mV are plotted in Fig. 3 as a function of inverse temperature. At all three biases the detector dark current is limited by diffusion currents for T > 60 K. At V_{det} = –50 mV, the detector dark current is limited by diffusion currents down to T ≈ 50 K. No generation-recombination currents are observed in these measurements and is consistent with previously reported data.[5,6] At V_{det} = –150 mV, T < 60 K and V_{det} = –100 mV, T < 50 K, the dark current has a negative temperature coefficient ($dI_{det}/dT < 0$) and the detector is limited by band-to-band tunneling.

R_oA_{imp} versus Temperature

R_oA_{imp} (A_{imp} is the detector p-n junction area) measurements were made as a function of temperature for a series of $Hg_{1-x}Cd_xTe$ detectors with x values ranging from x = 0.1925 to x = 0.3127. Modeled R_oA and measured R_oA_{imp} versus inverse temperature data is plotted in Fig. 4 for a $x_{opt} = 0.2981$ detector. The theoretical model[3] is a one-dimensional model that assumes diffusion currents are dominated by the n-side active layer and minority carrier recombination is via Auger and radiative processes. Input parameters for the model are the $Hg_{1-x}Cd_xTe$ layer x_{opt} value as determined from spectral response and thickness measurements, and carrier concentration from Hall data. The experimental R_oA_{imp} versus inverse temperature data displayed in Fig. 4 is parallel to the modeled R_oA versus 1/T calculation. Therefore, for this x_{opt} = 0.2981 case, $E_{a\ electrical} = E_{a\ optical}$ The large detector R_oA data being equal to the modeled R_oA versus 1/T calculation, indicates that the detector is limited by Auger and radiative processes.

The data displayed in Fig. 5 is similar to the data displayed in Fig. 4 for an x_{opt} = 0.1997 detector. A combination of $I_{det} - V_{det}$ curves and R_oA_{imp} versus inverse temperature data was used to calculate the temperature range within which the detectors are

diffusion limited. At temperatures greater than 100 K, the modeled R_oA line has a kink reflecting the inadequacy of the model in the intrinsic region. The measured data deviates such that the R_oA_{imp} versus inverse temperature slope at T is shallower than at low temperatures. This shallower slope is also caused by the detector now operating in the intrinsic region where the detector exhibits properties of a p-i device[7] with a dependence of qV/2kT. At temperatures between 100 K and 40 K, the R_oA_{imp} data is diffusion limited as explained in the previous section, there is no change in the slope at low temperatures to indicate any shift to generation-recombination current as the dominant current mechanism. However, as can be observed in Fig. 5, the slope of the measured electrical R_oA_{imp} versus inverse temperature data, is not equal to the slope of the modeled diffusion limited R_oA data. The activation energy $E_{a\ electrical}$ obtained from the measured R_oA_{imp} versus inverse temperature data displayed in Fig. 5 is,

$$E_{a\ electrical} = \beta * E_{a\ optical} \quad (2)$$

where $\beta = E_{a\ electrical}/E_{a\ optical} = 0.67$ in this case. $E_{a\ optical}$ is the activation energy calculated at 4 K using the x_{opt}

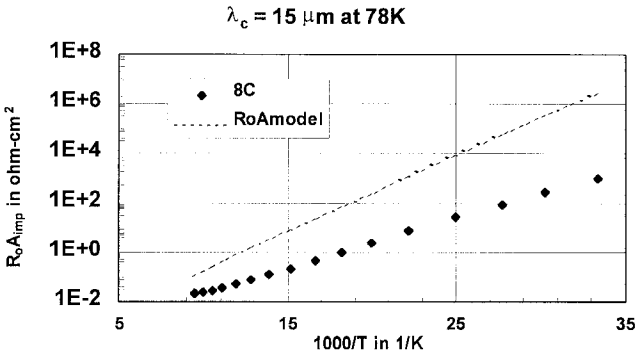

Fig. 5. R_oA_{imp} versus temperature for an 8 μm diameter detector from the same wafer as the detector in Fig. 1.

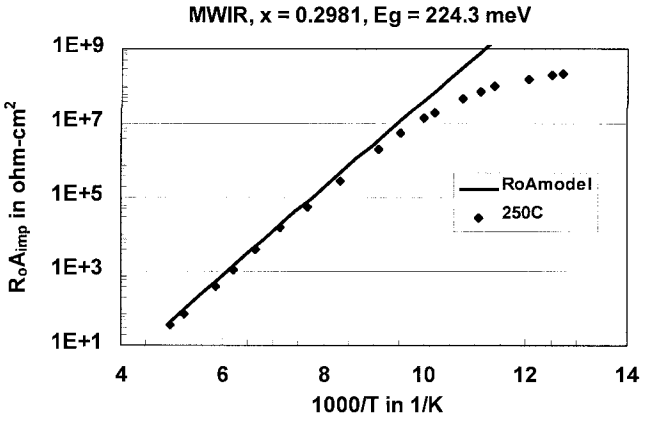

Fig. 4. R_oA_{imp} versus temperature for a 250 μm diameter, λ_c = 5.12 μm at 78 K detector .

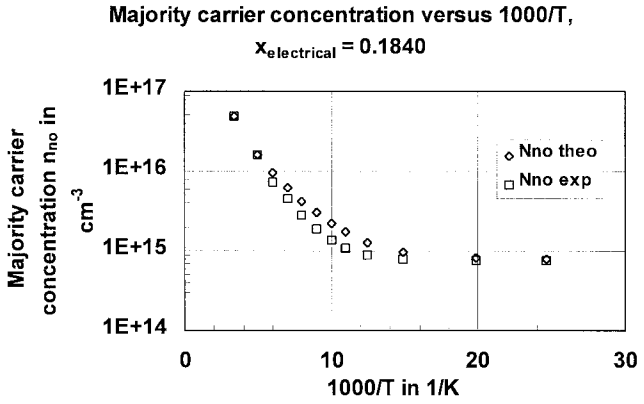

Fig. 6. Calculated and measured majority carrier concentration versus T, $x_{electrical}$ = 0.1840.

Table I. MWIR to VLWIR Wavelength Measured and Calculated Data

λ_c at 78 K in μm	x_{opt}	$E_{a\ optical}$ (T=4K) in meV	$E_{a\ electrical}$ in meV	β	$x_{electrical}$	$E_{a\ opt} - E_{a\ elect}$
17.4	0.1925	46.8	32.7	0.70	0.1843	14.03
17.0	0.1942	49.7	32.3	0.65	0.1840	17.38
17.0	0.1942	49.8	32.4	0.65	0.1841	17.40
16.2	0.1956	52.1	38.5	0.74	0.1877	13.53
16.2	0.1960	52.7	40.1	0.76	0.1888	12.66
15.0	0.1997	59.0	39.6	0.67	0.1883	19.48
15.0	0.2003	60.1	42.0	0.70	0.1897	18.02
14.2	0.2025	63.8	40.8	0.64	0.1890	22.96
12.8	0.2084	73.8	62.7	0.85	0.2019	11.07
12.1	0.2121	80.1	73.7	0.92	0.2083	6.41
11.8	0.2137	82.8	76.2	0.92	0.2098	6.62
10.8	0.2195	92.6	85.2	0.92	0.2151	7.41
10.8	0.2196	92.8	81.6	0.88	0.2130	11.13
10.1	0.2245	101.1	95.0	0.94	0.2209	6.07
9.7	0.2280	107.0	105.9	0.99	0.2274	1.07
6.8	0.2616	163.4	163.4	1.00	0.2616	0.00
5.1	0.2981	224.3	224.3	1.00	0.2981	0.00
4.8	0.3081	241.1	241.1	1.00	0.3081	0.00
4.7	0.3127	248.7	248.7	1.00	0.3127	0.00

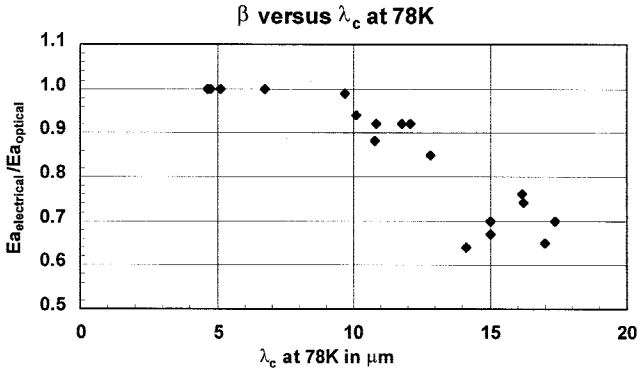

Fig. 7. $E_{a\ eletrical}/E_{a\ optical}$ versus λ_c.

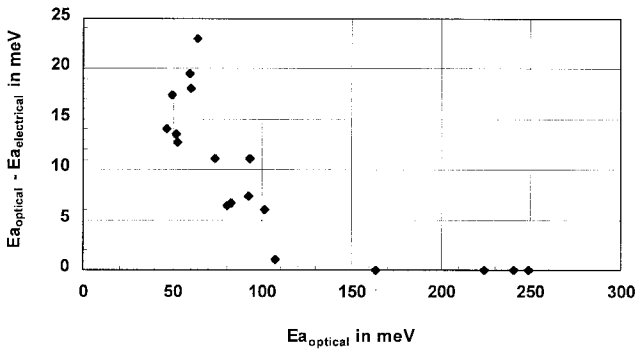

Fig. 8. ΔE in meV versus $E_{a\ optical}$ in meV.

value extracted from the spectral response curve and the expression listed in Eq. 1. Equation 1 is also used to extract x_{elect} values from $E_{a\ electrical}$.

Majority Carrier Concentration

Majority carrier concentration doped n-type with N_d = at 7.8×10^{14} cm^{-3} was measured as a function of temperature for a HgCdTe layer with $x_{optical} = 0.1942$ as determined from spectral response measurements. Using the measured majority carrier concentration at T = 300 K, the Hansen and Schmit[8] expression for intrinsic carrier concentration, Hansen, Schmit, Casselman equation[4] for bandgap and the Williams[3] model, an x = 0.1820 value is extracted from the models to match the measured majority carrier concentration at T = 300 K. The x = 0.1820 value is then used to calculate[3,8] the majority carrier concentration as a function of temperature and with the measured majority carrier concentration is plotted in Fig. 6 as a function of temperature. Deviations exist in the intermediate temperature range. The x = 0.1820 value extracted from the T = 300 K measurement is close to the $x_{electrical} = 0.1840$ value obtained from the $E_{a\ electrical}$ measured value.

DISCUSSION

Table I lists parameters extracted from measured data, the layers ranged from the MWIR to VLWIR wavelengths. Column 1 is the detector cutoff wavelength at 78 K. The x_{opt} values in Column 2 are obtained from the spectral response curves that include the effects of the active layer thickness. Therefore layers with the same cutoff wavelength at 78 K can have slightly different x values. Column 3 is the calculated cutoff wavelength and the bandgap $E_{a\ optical}$ at 4 K using the Hansen, Schmidt, Casselman Eq. 1. The activation energy $E_{a\ electrical}$ obtained from the R_oA_{imp} versus inverse temperature data is in Column 4. Column 5 is a list of the β values for all the layers. The values range from 0.64 to 1.0. A β value of 1.0 implies that the measured R_oA_{imp} versus inverse temperature data is parallel to the modeled diffusion limited data. Column 6 is the x_{elect} extracted from $E_{a\ electrical}$ using Eq. 1. Column 7 in Table I is a calculation of the difference $\Delta E = E_{a\ optical} - E_{a\ electrical}$ between the bandgap energy $E_{a\ optical}$ as measured from optical measurements described previously and $E_{a\ electrical}$ the activation energy extracted from the measured R_oA_{imp} versus inverse temperature data.

The ratio E_a/E_g is plotted versus the detector cutoff wavelength at 78K in Fig. 7. The data seems to fit to an equation

$$\beta = \frac{E_{a\ electrical}}{E_{a\ optical}} = 1 - \frac{(\lambda_c - 10)}{25} \qquad (3)$$

However, this is just an empirical fit to the data, no underlying physics information is obtained. What is clear is that the ratio β is not a constant as the cutoff wavelength (band gap) changes, it ranges from 0.64 to 1.0. This implies that the electrical measurements are not dominated by a midgap state or a state that exists at a fixed percentage of the gap as has been observed in SWIR detectors.[9] Figure 8 is a plot of bandgap difference ΔE_g versus $E_{a\ optical}$. There does not exist a constant ΔE for all the measured layers. Therefore there does not exist a defect level in the gap that is a fixed level of energy below the conduction band edge or above the valence band edge. The conjecture is that there exists band tailing of the density of states[10,11] into the gap that affects the electrical properties, giving rise to activation energies $E_{a\ electrical}$ that are smaller than the gap values $E_{a\ optical}$ obtained from optical measurements, the optical absorption coefficient between states in the band tails being low, and thus not contributing to the optical response of the detector. Therefore the observed behavior is related to the intrinsic properties of the material and not to discrete defect levels.

CONCLUSION

MWIR to VLWIR detectors have been characterized as a function of temperature to determine the dominant current mechanisms impacting detector performance. The detectors are diffusion limited near zero bias down to 40 K, the R_oA_{imp} versus temperature data thus representing the diffusion current performance of the detector as a function of temperature. In small ($E_{a\ optical}$ ~ 70 meV and lower) bandgap material, the activation energy $E_{a\ electrical}$, obtained from the measured diffusion limited R_oA_{imp} versus temperature data is not equal to the activation energy $Ea_{\ optical}$, obtained from the spectral response measurement.

What is obtained is, $E_{a\ electrical} = \beta^* E_{a\ optical}$, where β ranges between 0.64 to 0.75 for $E_{a\ optical} < 70$ meV. For large ($E_{a\ optical} > 200$ meV) bandgap material, $Ea_{electrical} = E_{a\ optical}$. As the band gap energy decreases to values in the range of 70 meV and lower, it is reasonable to expect a more dominant role of band tailing effects on the transport properties of the material system. It is expected that the optical band gap be unmodified, whereas the intrinsic concentration could be enhanced from its value for the ideal semiconductor. Such a picture could explain the observed behavior.

Additional work is needed to validate this hypothesis. Models that include the effects of band tailing and overlaying bands should be used to calculate intrinsic carrier concentration n_i and the optical/electrical properties of $Hg_{1-x}Cd_xTe$ material as a function of x. Measurement of $Hg_{1-x}Cd_xTe$ material with x values ranging from 0.15 to 0.22, are needed to correlate measured optical absorption coefficient, electrical conductivity, and intrinsic carrier concentration with modeled values.

REFERENCES

1. J.M. Arias, J.G. Pasko, M. Zandian, S.H. Shin, G.M. Williams, L.O. Bubulac, R.E. De Wames, and W.E. Tennant, *J. Electron. Mater.* 22, 1049 (1993).
2. J. Bajaj, J.M. Arias, M. Zandian, D.D. Edwall, J.G. Pasko, L.O. Bubulac, and L.J. Kozlowski, *J. Electron. Mater.* 25, 1394 (1996).
3. G.M. Williams and R.E. DeWames, *J. Electron. Mater.* 24, 1239 (1995).
4. G.L. Hansen, J.L. Schmit, and T.N. Casselman, *J. Appl. Phys.* 53, 7099 (1982).
5. R.E. DeWames, G.M. Williams, J.G. Pasko, and A.H.B. Vanderwyck, *J. Cryst. Growth*, 86, 849 (1988).
6. R.E. DeWames, J.G. Pasko, E.S. Yao, A.H. B. Vanderwyck, and G.M. Williams, *J. Vac. Sci. Technol.* A6, 2655 (1988).
7. J. Lindmayer and C.Y. Wrigley, *Fundamentals of Semiconductor Devi*ces (New York: Van Nostrand Reinhold Co., 1965).
8. G.L. Hansen and J.L. Schmit, *J. Appl. Phys.* 54, 1639 (1983).
9. R.E. De Wames, D.D. Edwall, M. Zandian, L.O. Bubulac, J.G. Pasko, W.E. Tennant, J.M. Arias, and A. D'Souza, *J. Electron. Mater.* 27, 722 (1998).
10. M.H. Cohen, H. Fritzsche, and S.R. Ovshinsky, *Phys. Rev. Lett.* 22, 1065 (1969).
11. N.F. Mott and E.A. Davis, *Electronic Processes in Non-Crystalline Materials,* Second Edition (Oxford, U.K.: Clarendon Press, 1979).